Advanced Steel Construction – Vol. 17 No. 4 (2021) 412–424
DOI:10.18057/IJASC.2021.17.4.10

SIMPLIFIED MODELLING OF NOVEL NON-WELDED JOINTS FOR MODULAR STEEL BUILDINGS

Kashan Khan [1], Zhi-Hua Chen [1, 2, 3], Jia-Di Liu [1, *] and Jia-Bao Yan [1, 3]

[1] *Department of Civil Engineering, Tianjin University, Tianjin, China*
[2] *State Key Laboratory of Hydraulic Engineering Simulation and Safety, Tianjin, China*
[3] *Key Laboratory of Coast Civil Structure and safety, Ministry of Education, Tianjin University, Tianjin, China*
** (Corresponding author: E-mail: jdliu@tju.edu.cn)*

ABSTRACT

Prefabricated modular steel (PFMS) construction is a more efficient and safe method of constructing a high-quality building with less waste material and labour dependency than traditional steel construction. It is indeed critical to have a precise and valuable intermodular joining system that allows for efficient load transfer, safe handling, and optimal use of modular units' strength. Thus, the purpose of this study was to develop joints using tension bolts and solid tenons welded into the gusset plate (GP). These joints ensured rigid and secure connectivity in both horizontal and vertical directions for the modular units. Using the three-dimensional (3D) finite element (FE) analysis software ABAQUS, the study investigated the nonlinear lateral structural performance of the joint and two-storey modular steel building (MSB). The solid element FE models of joints were then simplified by introducing connectors and beam elements to enhance computational efficiency. Numerous parameters indicated that column tenons were important in determining the joint's structural performance. Moreover, with a standard deviation (SD) of 0.025, the developed connectors and beam element models accurately predicted the structural behaviour of the joints. As a result of their simplification, these joints demonstrated effective load distribution, seismic performance, and ductility while reducing computational time, effort, and complexity. The validity of the FE analysis was then determined by comparing the results to the thirteen joint bending tests performed in the reference.

ARTICLE HISTORY

Received: 14 November 2020
Revised: 10 May 2021
Accepted: 10 May 2021

KEYWORDS

Novel joints;
Modular steel building;
Finite element analysis;
Simplified model;
Parametric study

1. Introduction

The construction of prefabricated modular steel (PFMS) structures makes use of modular blocks that are manufactured in the factory as corner-supported or load-bearing modules, transported to the site, and then installed into an MSB [1,2]. Offsite construction decreases construction period, waste generation, onsite noise and dust while increasing productivity, quality, and onsite worker safety [3,4]. The PFMS construction has become more important for new urban development than traditional onsite construction [5,6]. The connection mechanism, construction, and design are unique to PFMS, while the lower energy consumption, deadweight, and increased bearing capacity distinguish PFMS from conventional construction [7–9]. Because of its development and performance, the use of MSB in a repeated type of building has attracted construction companies' attention [10,11]. Based on the load transmission path, the MSB is primarily divided into two types. The first is load-bearing, which uses C-section walls to transmit gravity loads. In the second type, gravity and lateral loads are transferred to the base via corner posts [12,13]. Proper connections between interconnected modular units and lateral stabilising members, such as concrete core and corrugated plates, are necessary to withstand lateral forces [14,15]. Due to the increased number of connections in MSB, the resistance to collapse is exceptional; this results in increased structural integrity and alterative load transfer routes; if members sustain accidental damage [14,16]. Several previous studies reported intermodular connection techniques and evaluated their performance under lateral loadings. For instance, one study proposed a vertical intermodular connection via onsite welding of columns, while a horizontal connection via onsite clip bolting [8]. Then, a seismic design for a multistorey braced frame was proposed using these welded joints. However, complete welding of the joint is impossible, resulting in the upper and lower modules rotating differently. Additionally, braced frames greatly reduce lateral sway, which overestimates joint performance and results in an unrealistic load transfer mechanism. The seismic response of blind bolted beam-column joints was investigated through experiments, accompanied by their simplistic theoretical analysis in MSB. The study, however, did not address the lack of space for screwing bolts into interior modular units [17]. The seismic performance of a joint composed of a hollow steel box and a pre-tensioned threaded rod was determined through eight cyclic loading tests [18]. However, the study was limited to corner module joints and did not look into the impact of parametric variations on interior modular joints. Furthermore, static and cyclic load tests were performed to determine the structural performance of an MSB's cross-shaped cover plate joint. However, aside from column weakening caused by access holes, the difficulty of screwing the cover plate in the interior module was not addressed [19]. Several studies adapted the FE method to investigate newly formed MSB joints in addition to the experimental studies mentioned above [20,21]. For example, the axial compression and lateral performance of the VectorBloc joints were evaluated [22,23]. However, the study's findings were limited to corner modules in an elastic regime. It was also unable to discuss elastoplastic mode and the influence of adjacent modules by looking into interior modules. The self-locking interaction system was created to withstand shear forces in MSBs, and the robustness of the system was confirmed through dynamic analysis [5]. However, the joining system was unable to withstand tensile or bending forces. The fully-bolted joints using long beam bolts and column bolts were developed for low-storey MSB [24]. Their seismic performance was investigated using FE analysis, followed by the simplification to conduct dynamic analysis on multistorey buildings [25,26]. Similarly, in addition to joint studies, researchers used finite element models to analyse the rigidity of individual and combined modular units with corrugated walls subjected to lateral loads and contribute to making design recommendations [27]. However, because the study focused on corrugated shear walls as the primary lateral stabilising members, the study prioritised their performance, and seismic behaviour of joints was avoided by simplifying them. It is evident that the majority of previous studies identified joints for cold-formed or C-sections or joints that required access holes in columns or beams to operate bolt screwing, resulting in a weakened cross-section or joints unable to connect interior modules. Similarly, most studies concentrated primarily on the lateral performance of corner frames and the development of simplified models for them, ignoring the actual performance of middle and interior joints, as well as the rotational stiffness of intermodular joints [28–30]. Furthermore, the majority of simplified models were capable of simulating joint elastic behaviour without accounting for elastic-plastic performance. Simultaneously, few studies have investigated the lateral performance of complex forms of modular frames or modular blocks; however, the influence of adjacent bare frames and intermodular joints was not considered. Thus, the current study intended to examine the behaviour of various types of joints, such as corner, middle, and interior joints, and to develop simplified models of these joints for use in future practical engineering applications. Following this, extensive parametric analysis was performed, as well as the application of the developed simplified models in modular units to determine their computational efficiency and accuracy in MSB.

As a result, a new type of joint for connecting hot-rolled structural hollow sections (SHS) with superior torsional resistance is being developed in this study. These joints can avoid compromising the bearing capacity of the structural members by creating access holes or using weaker structural

C-sections. At the same time, they can also maintain an aesthetically pleasing appearance by avoiding diagonal stiffening plates on columns and beams to prevent brittle weld failure between them. The lateral structural performance of these joints and their detailed simplifications with the connector and beam-element model has been researched using FE software ABAQUS. The developed simplified models can simulate the elastoplastic behaviour of corner, middle and interior joints in MSB. The accuracy of FE analysis results is validated by comparing them to similar experimental studies [31–33]. These analyses lead to a more profound indulgence of the joint's behaviour and their contribution to an MSB.

2. Detailing and force transfer mechanism of joint

Fig. 1(a) describes an MSB with various connection systems, while Fig. 1(b) depicts the assembly of SHS members with established joints (b). Modules are produced by welding columns and beams to the upper and lower parts of joints. In contrast, the middle part (tenons with welded GP) and tension bolts are used for the horizontal and vertical combination of adjacent modular units to form an MSB. The dimensions of the joint components are illustrated in Fig. 2(a). Because the depth of the floor beam is slightly more than the ceiling beam; therefore, the length of the middle tenon is more above than below the GP.

The vertical and lateral loads applied to an unbraced multistorey MSB with a clear storey height of h are depicted in Fig. 2(b). The intermodular space is preserved to facilitate module assembly and allow for the passage of MEP systems through the MSB during its life cycle. When vertical and lateral loads are applied, the deflected shape of the unbraced multistorey frame with its inflection point is highlighted. The lengths of the columns and beams are then determined in the MSB using these contra flexure points. The centreline distances of the subassembly are determined using the column's mid-height (h/2) and the beam's mid-length (L/2). Furthermore, these unbraced frames' displacements and sidesway directions are denoted as positive (+Δ) and negative displacement (-Δ). Since the moment distribution capacity of a vertical intermodular connection is dependent on their moment capacity (M_0) in these semi-structured unbraced frames, this capacity has to be deducted in this study. Whereas beam-column welded intramodular connections are fabricated using the fillet welding process, so they are considered rigid.

The upper column is assumed to be free to facilitate sidesway of the unbraced frame. The bottom column was pinned, allowing the base rotation while preventing its translational; however, the upper column's sidesway was maintained. Beams were supported by sliding roller boundary conditions, allowing for lateral displacements and in-plane rotation in the event of a sidesway.

The load transfer mechanism of the joint in its practical application in unbraced MSB against combined lateral loads, such as wind, earthquake, and gravity, is illustrated in Fig. 2(c). The detailed FE analysis determined that when the lateral load (V) and the vertical load (P) is applied at the middle top of the modular columns, the lateral displacement can be measured as a sidesway, such as Δ_c in columns and Δ_b in beams. At the same time, columns and beams bend against joint tenons, resulting in the columns and beams resisting shear stresses (i.e., V_c and V_b) while resisting bending moments (i.e., M_c and M_b). Additionally, joints resist bending moments in proportion to their moment capacity (M_0) in the upper and lower modules. The connection bolts are primarily subjected to slight tension forces, which result in a gap formed between the upper and lower components.

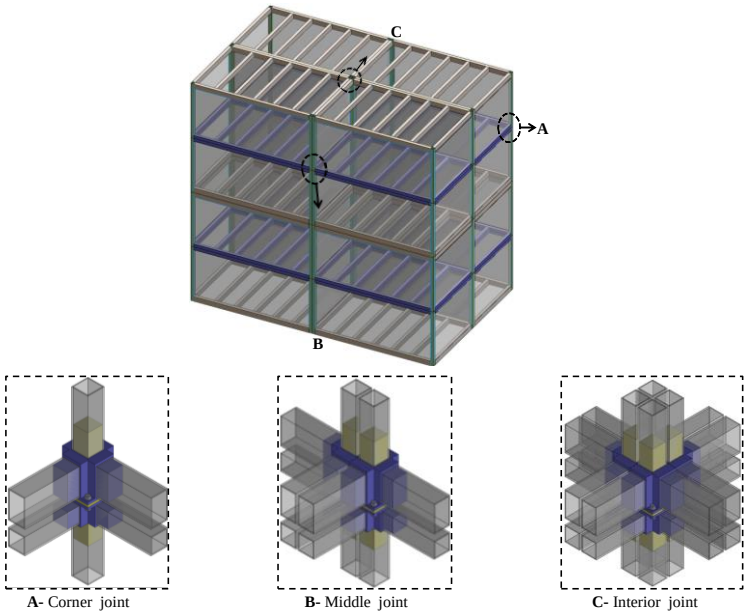

(a) Details of joints in MSB

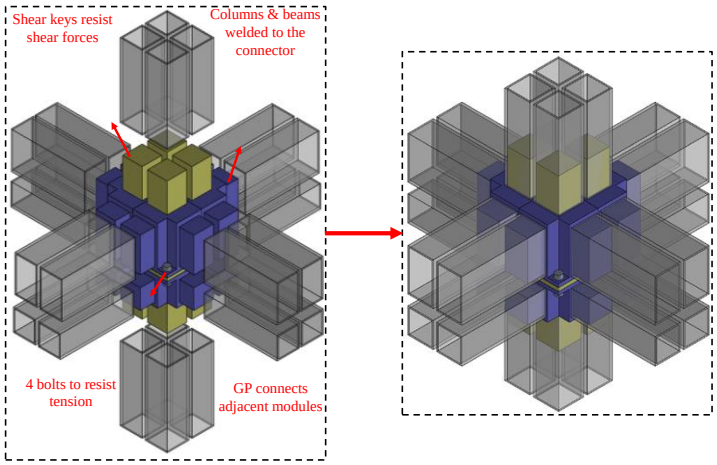

(b) Assembly of the newly developed joint

Fig. 1 A developed joint connecting mechanism in an MSB

3. Experimental studies on joints in MSB

Previously conducted research examined the seismic behaviour of corner and middle joints under static and cyclic loading conditions. The structural behaviour of the joints was compared when diagonal stiffeners were used versus when they were omitted. The joints were created by hollow plugins and screwing long beam bolts to support the upper and lower modules [31,32]. Additionally, the rotational stiffness of the rotary joint was examined [33]. The current study validated the FE analysis and conducted additional nonlinear finite element analyses on a joint developed in this study using the experimental findings from the studies mentioned above.

3.1. Test details

The joint design in the studies mentioned above was compatible with the main author's five-storey MSB project in Tianjin, China. The experiments' primary objective was to evaluate the joints' nonlinear structural performance, load-bearing capacity, seismic response, and rotational rigidity. All tests were conducted at Tianjin University's Structural Engineering laboratory. The static and quasi-static loadings, the effect of diagonal stiffening plates, the beam cross-section, and axial force ratios (AFR) were taken into account. Under static load, the ultimate capacities and failure mechanism of two corner and middle frames with and without stiffeners were investigated. Four additional specimens of the corner and middle frames were subjected to cyclic loading to assess joints' energy consumption and seismic behaviour. The four specimens that were not stiffened were considered standard, whereas the remaining eight specimens that were stiffened were considered parametric. The column end loading technique was adapted to apply the 100t force to the upper free column, with the floor beam (FB), ceiling beam (CB), and lower column supposed to act as the rotational hinge. The experiments used the Chinese standard (JGJ101-96) for cyclic loading [31,32]. Similarly, the rotary joint was used in another MSB project (Ziya Shanglinyuan) in Tianjin, China; thus, the mechanical properties of the joint were similar to those of the actual project. However, the study treated the rotary fitting as a regular bolt [33].

3.2. Material properties

Mild steel Q345B was used for columns, floor beams, ceiling beams, cover plates, diagonal stiffening plates, and beam bolts. On the other hand, joint components were made of cast steel, including ZG35, G20Mn5QT, and ZG310-570. The columns and beams were welded using groove welds, while the stiffeners were welded using fillet welding. Table 1 contains a list of material properties for structural components (i.e., symbols S/SC/QS denote joints with the plugin, while TS denotes rotary joint) that were evaluated compared to the materials used in actual MSB projects.

Table 1
Test specimens' material properties

Type of sp.	Structural Component	Thickness (mm)	Yield strength f_y(MPa)	Ultimate strength f_u(MPa)	Elongation in % age
S/SC/QS	Column, beam plate	8	425	575	30
-	Stiffeners	16	350	510	26
-	Cast plugin device	-	330	350	22.5
TS	Column	18	410	575	26
-	Corner fitting	16	355	515	32.5
-	Connecting plate	-	390	560	35
-	Rotating part	-	340	590	18

4. Numerical modelling technique

4.1. General

ABAQUS/CAE was used to develop FE models, while ABAQUS/Standard type solver was used for nonlinear analysis of detailed solid element and simplified beam element models [34]. The samples used to examine the lateral response of the joints developed in the study are listed in Table 4. The FE models included columns, beams, tension bolts, and joint components.

4.2. Materials model of steel

A nonlinear isotropic/kinematic hardening model is used for all structural members. The model is an elastic-plastic isotropic model that uses the von Mises yielding criteria to define isotropic yielding. For the columns, beam members, and mid-part of the joint, the FE simulation uses Q345B mild steel material properties obtained from the previously mentioned test studies. The upper and lower joint parts, on the other hand, are made of ZG35 cast steel. Tensile stress-strain behavioural patterns of structural steel use a three-linear stress-strain behaviour that takes strain hardening into account, as shown in Fig. 2(c). [35]. Elastic material properties such as Poison's ratio "ν" and modulus of elasticity "E_s", whereas plastic material properties such as yield strength "f_y", ultimate strength "f_u", and strain values "ε" for SHS members and joints are listed in Table 1. Engineering stress and strain are described in Table 1, whereas true stress and strain are inputted in ABAQUS. Consequently, Eqns. (1) and (2) are introduced to convert engineering stress and strain to true stress and strain.

$$\sigma_T = \sigma_E(1 + \varepsilon_E) \tag{1}$$

$$\varepsilon_T = \ln(1 + \varepsilon_E) - \frac{\sigma_T}{E_s} \tag{2}$$

where, σ_T and σ_E denote true and engineering stress, while ε_T and ε_E indicate true and engineering strain.

4.3. Formation of the FE model

To resolve convergence issues, reduce contact surfaces, and improve computational efficiency, numerous simplifications are made to the FE modelling, including circular modelling of bolt heads and nuts, ignoring threads on bolts and nuts, and overlooking spaces between bolts and bolt holes. The welded cover plates, stiffening plates, and beam-column frame skeleton is modelled as a single part for validation purposes, resulting in improved accuracy and fewer complications.

4.3.1. Mesh technique

High-order contact analysis on three-dimensional deformable solid parts such as SHS members and joint components was performed using hexagonally structured mesh controls with an eight-node linear brick, reduced integration, and Hourglass Control Element Type (C3D8R). Corners and areas with geometrical changes, joint regions, bolts, bolt holes, and other high-stress areas and components were finely meshed. The most reliable validation of FE with test results was achieved using four different mesh densities: very fine, fine, coarse, and very coarse. Then the most precise mesh density was used. To simplify FE models, columns and beams had been substituted with three-dimensional beam elements with cross-sections similar to those of detailed solid elements. The beam element sections were meshed using a two-node linear beam element (B31) and the same mesh size as the detailed models.

4.3.2. Contacts and interactions properties

The contact between the column and the tenon, the beam and the tenon, and the joints and bolts were simulated as surface-to-surface contact (standard), with "hard contact" as the normal behaviour and "finite sliding" as the tangential behaviour through the use of the "penalty friction formulation." The hard contact formulation allows two contacting surfaces to share pressure while they are in contact, but no pressure transfer occurs after the contact surfaces are separated. Alternatively, the penalty friction formulation uses a friction coefficient to account for the relative motion of the contact surfaces and calculate the frictional force. After validating the FE results with experimental data, an accurate friction coefficient was chosen. The interaction between columns, beams, and neighbouring joint faces was modelled as hard contact in middle and interior frame samples to maintain consistent force transfer between neighbouring modules. Because columns and beams were welded to their respective joint components, the "Tie constraint" was used to model the interactions between a column and joint and a beam and joint. A tie constraint is a connection between the two distinct surfaces that prevents them from moving relative to one another. The fusion of two regions is achievable with this constraint, even if the meshes created on their surfaces are different.

4.3.3. Boundary conditions and loading mechanism

The study used the test arrangement outlined in the previous studies and the sway frame criteria described in Fig. 2(b) to analyse the nonlinear lateral performance of joints. Therefore, the movement of the lower column at the bottom was restricted in all directions. In contrast, the upper column only restrained out-of-plane movement, and beams were restricted in the vertical and

out-of-plane directions. Besides, the out-of-plane rotation of beams was restricted, allowing them to exhibit only in-plane rotation. The upper column was subjected to lateral displacement-controlled loading as a predicted sidesway and vertical axial loading as a percentage of the column's designed bearing capacity, as calculated from Eqn. (1) to observe the elastoplastic behaviour and simulate the actual force transmission of members in unbraced MSB [36]. Additionally, floor beams were subjected to a factored dead load as the structure's self-weight and a live load calculated according to ASCE 7-10 to investigate the nonlinear lateral bearing capacity of a multistorey modular block with developed joint [14,37]. Furthermore, the modular block's base was assumed to be fixed, while displacement-controlled loading was applied to the middle of the ceiling beam along the modular block's longer direction [38]. During the validation of FE simulation, the following Eqn. (4) was used to predict the pretension force of beam bolts.

$$N = (AFR) f_{yc} A_s \tag{3}$$

$$P = \frac{(0.9)^3}{1.2} A_e f_{tv} \tag{4}$$

where, N denotes the axial load, AFR denotes the axial force ratio, A_s denotes the area of the column, P denotes the bolt's pretension force, A_e denotes the bolt's effective area, and f_{tv} denotes the bolt's tensile strength, which is taken as180 MPa.

4.3.4. Failure criteria in FE modelling

The ABAQUS library included stress criteria and total equivalent plastic strain (PEEQ) criteria for analysing the yielding or fracture condition of ductile material and the distribution of plastic or permanent strain [39]. The equivalent stress and plastic strain were specified as follows:

$$\sigma_{EQ} = \sqrt{\frac{(\sigma_1-\sigma_2)^2+(\sigma_2-\sigma_3)^2+(\sigma_3-\sigma_1)^2}{2}} \tag{5}$$

$$\text{PEEQ} = \int_0^t \sqrt{\frac{2}{3}\dot{\varepsilon}_{ij}^p \dot{\varepsilon}_{ij}^p}\, dt \tag{6}$$

where, σ_{EQ} stands for von Mises stress or equivalent stress; σ_1, σ_2 and σ_3 stand for principal stresses; PEEQ stands for permanent strain, and $\dot{\varepsilon}_{ij}^p$ stands for rate of plastic strain.

4.3.5. A convergence of FE simulation

The experimental results were used to determine the exact solution for FE analysis convergence to obtain the value with the smallest error tolerance. The convergence study took into account strain hardening, bolt friction, mesh sizes, and friction coefficients. As shown in Table 2, specimen S1 was chosen for strain hardening, QS4 for bolt friction, and SC1 for four different mesh sizes and friction coefficients.

The load-carrying capacities of FE models with varying convergence criteria were compared in Fig. 3. Fig. 3(a) illustrates the initial stiffness, yielding, and load-carrying path for models with and without strain hardening. The figure illustrates that strain hardening increased the model's bearing capacity. However, the increase in ultimate bearing capacity observed was only 1%. Similarly, using the same loading criteria, two models were used to analyse the bolt friction. As shown in Fig. 3, a pretty small change in load-carrying capacity of 0.006% was observed when bolt friction was included in the FE model. Additionally, four models with very fine, fine, coarse, and very coarse mesh densities were analysed against lateral loading using sizes of 25, 30, 40, and 50 mm. It was found that as the mesh expanded from very fine to coarse, the ultimate strength increased too. Nevertheless, the very coarse mesh demonstrated a slight reduction in capacity compared to the coarse mesh model, as illustrated in Fig. 3(c). However, no recognisable discrepancy in capacity was observed between coarse and very coarse mesh density models. In contrast, a model with a very fine mesh was incapable of sustaining a load greater than 73 mm, resulting in non-convergence. A fourth convergence study was conducted on friction coefficients. Finite element models with four different values, 0.3, 0.4, 0.5, and 0.6, were analysed, and Fig. 3(d) demonstrated that models with a higher friction coefficient had a greater bearing capacity. Moreover, the capacity increase between modelling techniques with friction coefficients of 0.3 and 0.6 was only 1.5%.

Based on a detailed analysis of the different convergence criteria and the test results, strain hardening was taken into account, but bolts were modelled as frictionless. The structural components have meshed with a 30 mm size, the joint region with a 10 mm size, and the hole area with an 8 mm size. Moreover, the friction coefficient was set to be 0.3.

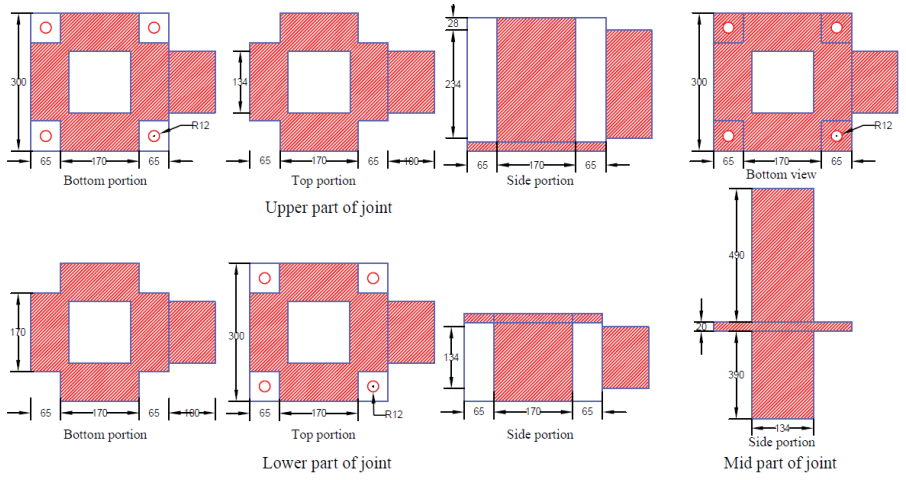

(a) Dimensions of the developed joint (unit: mm)

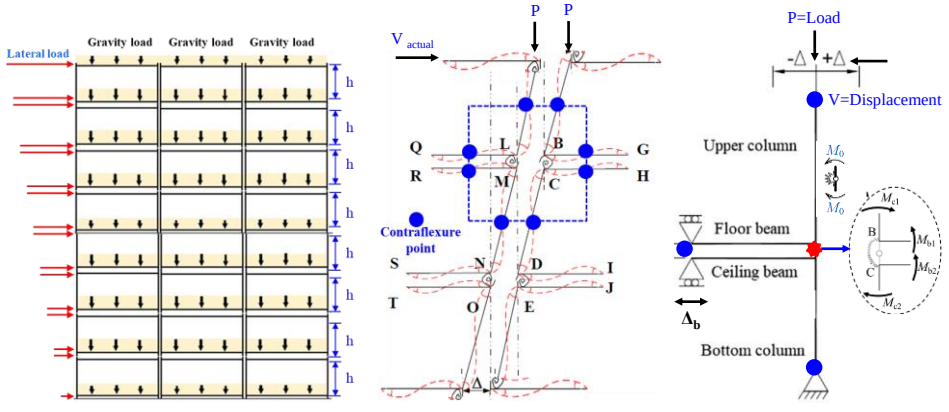

(b) Forces transfer mechanism & frame classification in MSB

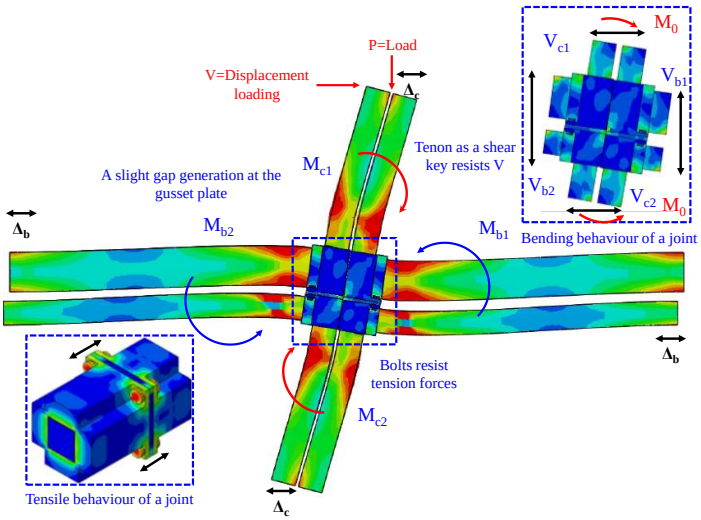

(C) Forces transfer mechanism of the developed joint unbraced MSB (deflection scaled 5times)

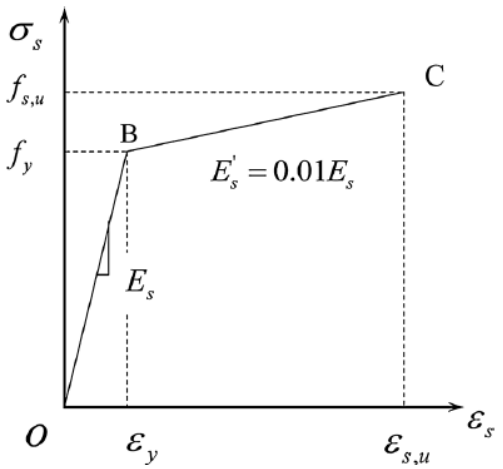

(d) The true bi-linear elastic-plastic material model used in FE analysis [35]

Fig. 2 Forces transfer & material model details for joints in a FE study

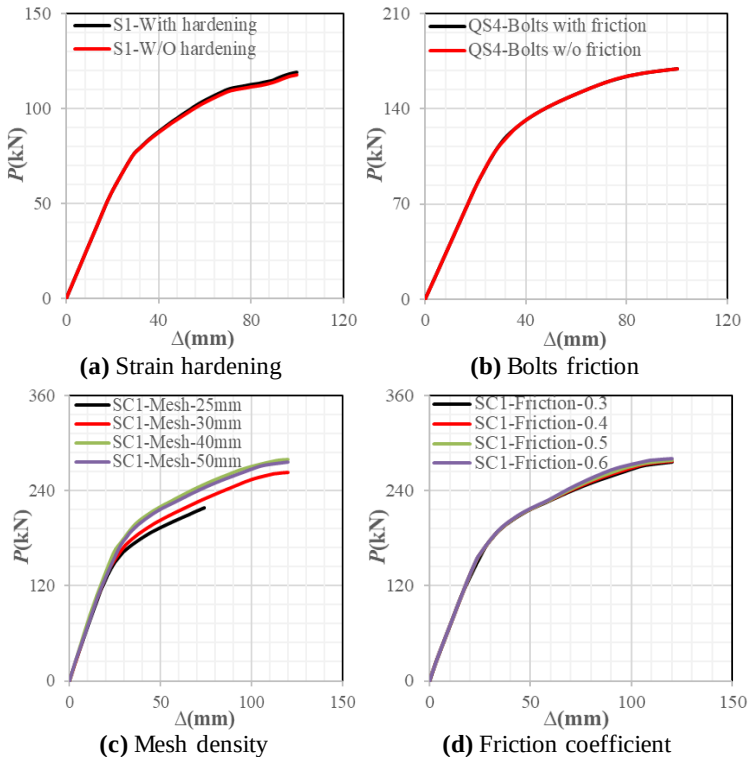

(a) Strain hardening **(b)** Bolts friction

(c) Mesh density **(d)** Friction coefficient

Fig. 3. Comparison of load-displacement curves obtained from convergence studies

Table 2
Detailing of test specimens

Sp. No	Type of joint	CB (mm)	FB (mm)	Column (mm)	Stiffener size (mm)	Bolt (mm)	AFR	Load application
S1	Exterior	150x150x8	150x250x8	150x150x8	None	24	0.2	Static
SC1	Interior	150x150x8	150x250x8	150x150x8	None	24	0.2	Static
S2	Exterior	150x150x8	150x250x8	150x150x8	10	24	0.2	Static
SC2	Interior	150x150x8	150x250x8	150x150x8	10	24	0.2	Static
QS1	Exterior	150x150x8	150x250x8	150x150x8	None	24	0.2	Cyclic
QSC1	Interior	150x150x8	150x250x8	150x150x8	None	24	0.2	Cyclic
QS2	Exterior	150x150x8	150x150x8	150x150x8	10	24	0.2	Cyclic
QSC2	Interior	150x150x8	150x150x8	150x150x8	10	24	0.2	Cyclic
QS3	Exterior	150x150x8	150x250x8	150x150x8	10	24	0.2	Cyclic
QSC3	Interior	150x150x8	150x250x8	150x150x8	10	24	0.2	Cyclic
QS4	Exterior	150x150x8	150x250x8	150x150x8	10	24	0.1	Cyclic
QSC4	Interior	150x150x8	150x250x8	150x150x8	10	24	0.1	Cyclic
TS	Corner	-	-	200x200x18	-	-	-	Bending

4.4. Validations of FE simulation

The results of FE static analysis were compared to the *P-Δ* relationships and failure events of test specimens (such as S/SC/QS/QSC) of plugin joints against static (four models) and cyclic (eight models) loadings. As shown in Table 3, the lateral load resistance of a rotary corner joint specimen (TS) was also validated.

4.4.1. Validations of bending test results with FE analysis

Finite element analysis results were compared to the lateral *P-Δ* curves of twelve test specimens of plugin joint and moment-rotation curves of a rotary joint, as shown in Fig. 4. The results of cyclic loading tests on plugin joint envelope curves were compared to the results of static FE analysis. It was discovered that FE models accurately simulated test specimens' ultimate capacity, stiffness, and ductility. There have been some discrepancy and inconsistency on a minor scale in stiffness or strengths between test and FE. This could be because of differences in material models, sectional imperfections during production, soft supports, or simplifications to the FE model.

Experiment failure modes were compared to von Mises stress distributions in FE models, as illustrated in Fig. 5. Gap development and enlargement, slicing of column or beam welds, stiffener breakdown, local column buckling, and beam tearing were the primary failure events in plugin joint test specimens. The stress localisations observed in FE models, including corner and middle joints, exhibited outward and inward buckling, high stress welded areas and gap generation that was entirely consistent with test results. Similarly, the test results were accompanied by accurate simulations of gap generation of 25 mm between corner fittings and their outward buckling, such as the gap generation of 27 mm demonstrated by FE models for rotary joints.

The comparison of the capacities of the tests specimens and FE models are shown in Table 3. It demonstrates that the average test-to-FE ratio (mean) and coefficient of variation (Cov) are 1.02 and 0.12, respectively. Table 1 summarises the ultimate compressive strengths predicted by the Test-to-FE prediction ratios, indicating that when the ratios exceed 1.0, the FE was marginally underestimated, implying that structural behaviour predictions are secure. Conversely, ratios less than 1.0 indicate that actual behaviour is overestimated, implying that structural behaviour estimations are unsafe. Hence, these comparisons of *P-Δ* curves and predicted P_u values demonstrate that FE analysis can accurately simulate lateral structural performance for newly developed joints and modular blocks when both axial compression and lateral loading are applied. As a result of the FE simulation's accuracy and efficiency, it is recommended to conduct additional parametric studies on joints and a modular block.

Table 3
Comparison of test specimens and FE models' ultimate capacities

Sp. No	Type of joint	Load application	Ultimate load (Test)/P_{Test}(kN)	Ultimate load (FE)/P_{FE}(kN)	P_{Test}/P_{FE}
S1	Corner	Static	112.0	118	0.95
SC1	Middle	Static	248.0	262	0.95
S2	Corner	Static	183.0	162	1.13
SC2	Middle	Static	396.0	392	1.01
QS1	Corner	Cyclic +ve	81.0	79	1.02
		Cyclic -ve	-102.0	-118	0.86
QSC1	Middle	Cyclic +ve	205.0	261	0.79
		Cyclic -ve	231.0	263	1.13
QS2	Corner	Cyclic +ve	118.0	121	0.97
		Cyclic -ve	-137.0	-127	1.07
QSC2	Middle	Cyclic +ve	255.0	261	0.98
		Cyclic -ve	-305.0	-260	1.17
QS3	Corner	Cyclic +ve	161.0	122	1.32
		Cyclic -ve	-183.0	-162	1.13
QSC3	Middle	Cyclic +ve	329.0	391	0.84
		Cyclic -ve	-364.0	-389	0.94
QS4	Corner	Cyclic +ve	141.0	129	1.09
		Cyclic -ve	-168.0	-169	0.99
QSC4	Middle	Cyclic +ve	377.0	387	0.97
		Cyclic -ve	-411.0	-388	1.05
TS	Corner	Bending	33.74.0	33.80	0.99
Mean					1.02
Cov					0.12

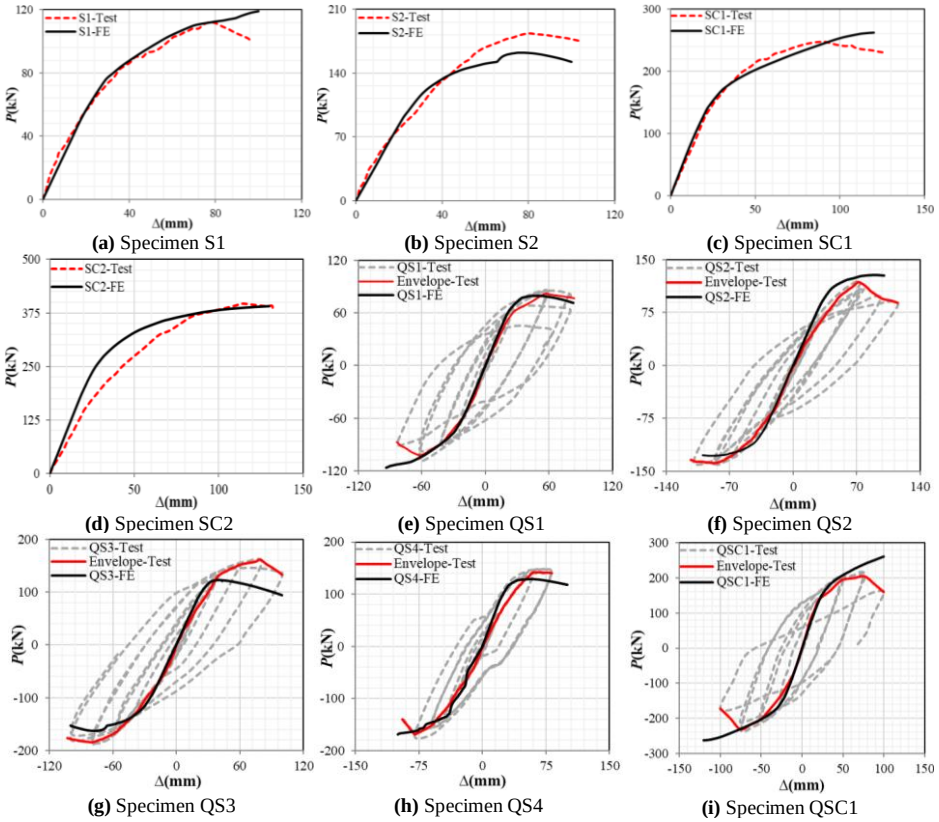

(a) Specimen S1 **(b)** Specimen S2 **(c)** Specimen SC1

(d) Specimen SC2 **(e)** Specimen QS1 **(f)** Specimen QS2

(g) Specimen QS3 **(h)** Specimen QS4 **(i)** Specimen QSC1

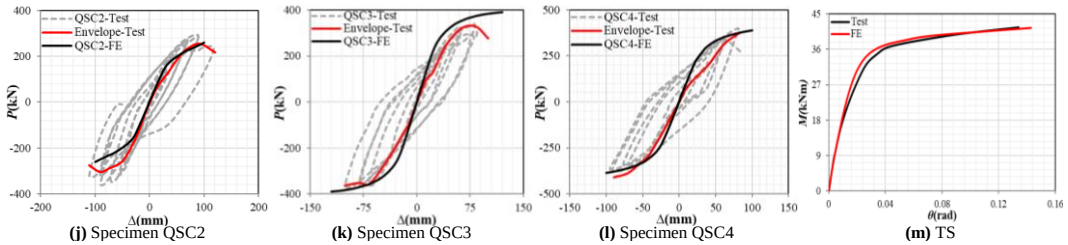

(j) Specimen QSC2 **(k)** Specimen QSC3 **(l)** Specimen QSC4 **(m)** TS

Fig. 4 Validation curves of FE models and test specimens

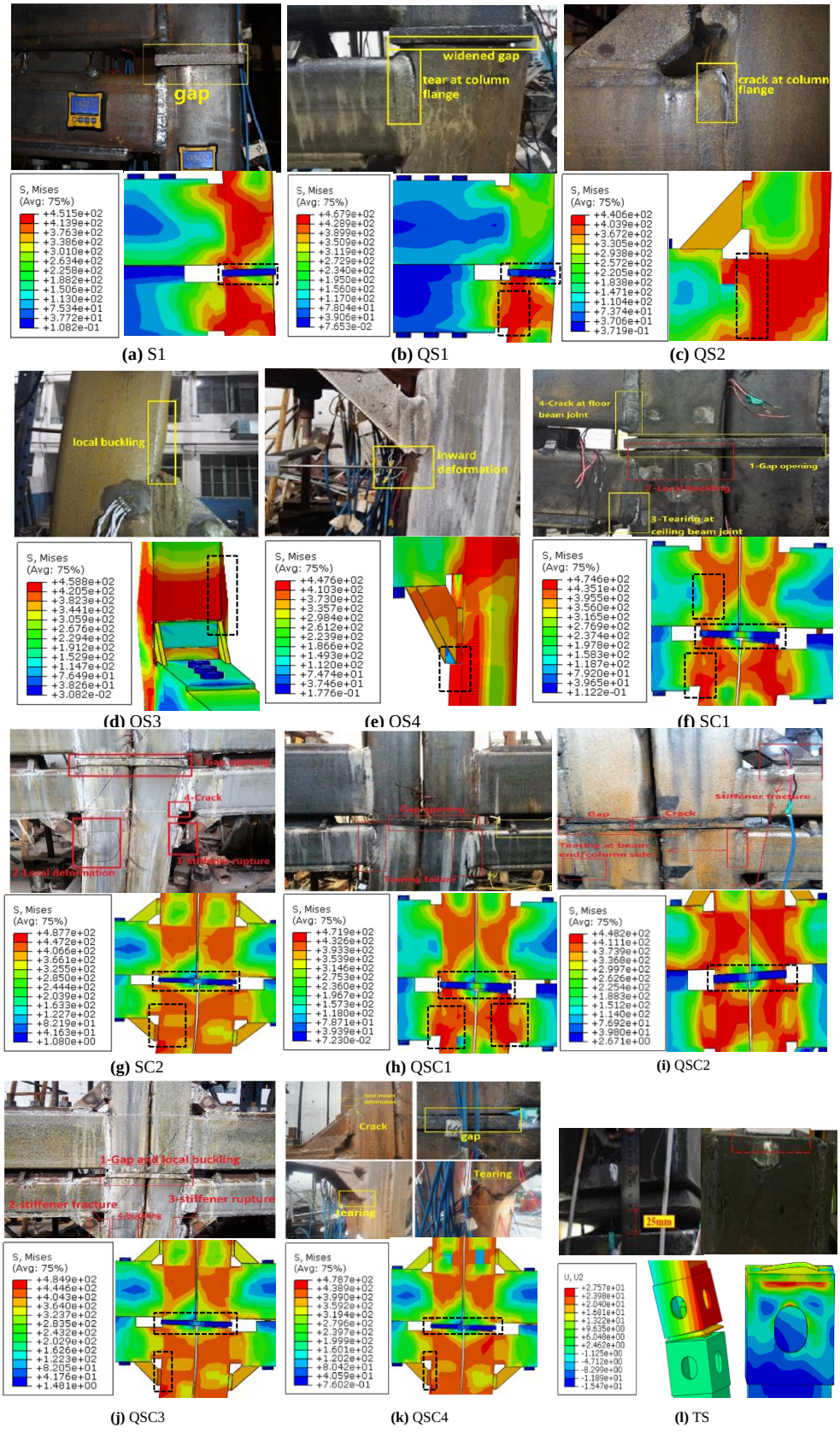

(a) S1 **(b)** QS1 **(c)** QS2

(d) OS3 **(e)** OS4 **(f)** SC1

(g) SC2 **(h)** QSC1 **(i)** QSC2

(j) QSC3 **(k)** QSC4 **(l)** TS

Fig. 5 Validation of failure modes of FE models and test specimens

Table 4
Details of FE models for lateral behaviour of the developed joint

Sp. No	CB (mm)	FB (mm)	Column (mm)	Bolts (mm)	AFR (%)	Loading method
S1	150x150x8x1900	150x250x8x1900	150x150x8x1000	24	0.2	Static
S2	150x150x8x1900	150x250x8x1900	150x150x8x1000	24	0.1	Static
S3	150x150x8x2900	150x250x8x2900	150x150x8x1000	24	0.2	Static
S4	150x150x8x1000	150x250x8x1000	150x150x8x1000	24	0.2	Static
S5	150x250x8x1900	150x250x8x1900	150x150x8x1000	24	0.2	Static
S6	150x150x8x1900	150x150x8x1900	150x150x8x1000	24	0.2	Static
Block-S	150x150x8x1000	150x250x8x1000	150x150x8x1000	24	-	Static
Block-L	150x150x8x3000	150x250x8x3000	150x150x8x1000	-	-	-

5. FE studies on the joints in MSB

5.1. Geometry and detailing

The joint assembly and dimensions of each component used in performance evaluation are depicted in Figs. 1(b) and 2(a). The structural performance of MSB with the established joint is evaluated using a small-scale two-storey modular block scaled to the recommended size. The specimens and structural components are described in detail in Table 4.

5.2. Bending behaviour of the joints

5.2.1. Corner joint

Six FE models of the corner joint supporting an upper and lower modular unit were analysed with varying AFR, beam lengths, and beam cross-sections. Fig. 6 shows that S6 exhibited the lowest bending moment capacity and initial stiffness, whereas S2 showed the largest bending capacity, and S4 exhibited the highest initial stiffness. It was found that an increase in the cross-sections of the beams increases bending capacity and vice versa, whereas the decrease in beam lengths increases the stiffness of the joint. Comparing the permanent plastic strain of models in Fig. 7(a) declares that all other models showed permanent allocation of strain in the upper column except specimen S6 (demonstrated strong column-weak beams). All models demonstrated different plastic strain distribution in FB, but S6 showed the failure of both beams, whereas S5 lacked beams yielding due to stiffer and stronger beams.

5.2.2. Middle joint

For studying the detailed bending performance of the middle joint, six models were analysed supporting four modules, such as two uppers and two lowers. Axial compression and lateral displacement loads were applied to the centre of the upper columns. In comparing the moment-rotation curves of models, the middle joint models behaved similarly to that of the corner joint, both in bending moment capability and initial stiffness, as shown in Fig. 6. The capacity and stiffness were increased by increasing the cross-section (model S5) and reducing the lengths of beams (model S4), which can be considered an upper bound. Meanwhile, reducing the cross-section (model S6) and lengthening of beams (model S3) reduced capacity and stiffness and can be regarded as a lower bound. Whether failure occurred in beams or columns, the effective distribution of stresses to adjacent members on the opposite side was evident, implying that the joint between adjacent modules performed effectively.

5.2.3. Interior joint

The bending capacity of six interior joint models supporting eight modular units was analysed. The upper four columns' centre was subjected to axial and lateral loads. The interior joint specimens all exhibited the same patterns of bending capacities and stiffness as the corner and middle joints. However, the capacities and stiffnesses of models S1 and S2 were slightly different from those of other models. Model S2 demonstrated a greater bending capacity than S1 but a lower stiffness than S1. The relationship between stiffness and capacity was more pronounced in interior joints than in corner and middle joints. Models S4 and S5 demonstrated the highest bending capacities and stiffnesses, while S3 and S6 demonstrated the lowest. As illustrated in Fig. 7, model S3 encountered stresses in the beams, preventing the load-taking operation from continuing. Except for S4 and S5 (which demonstrated high capacity and rigidity), all specimens indicated beam failure; however, equivalent stress propagation was observed in other structural components.

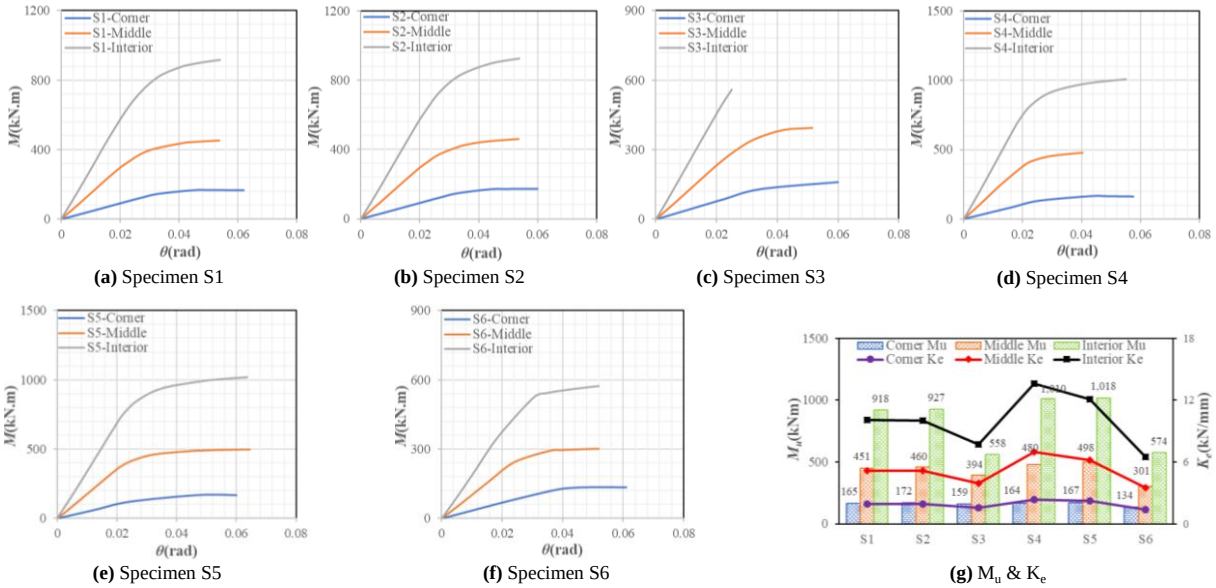

(a) Specimen S1 **(b)** Specimen S2 **(c)** Specimen S3 **(d)** Specimen S4

(e) Specimen S5 **(f)** Specimen S6 **(g)** M_u & K_e

Fig. 6 Moment versus rotation curves and scatters of FE models of joints

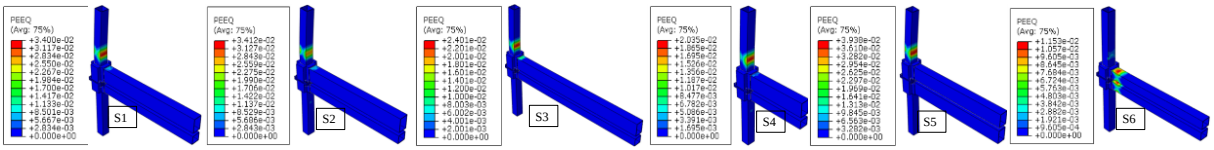

(a) Corner joint

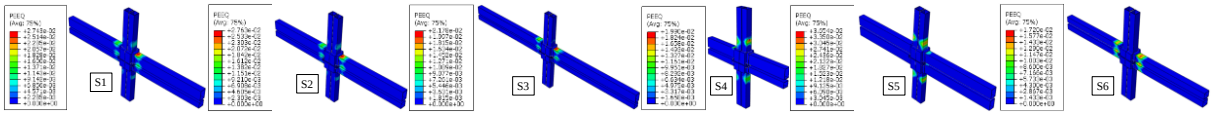

(b) Middle joint

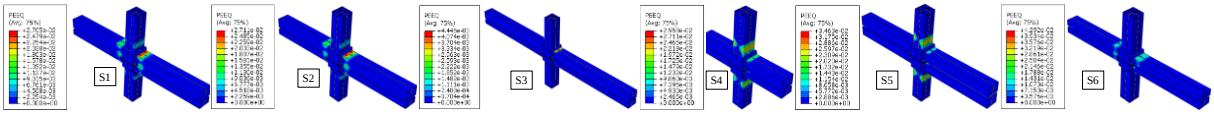

(c) Interior joint

Fig. 7 Plastic strain distribution of joints against lateral loads

5.3. Seismic performance of joints

The seismic performance of each joint model was evaluated using the special moment frame (SMF) parameters, which were found to be consistent with the 0.04 rad rotational deformation capacity with a strength of $0.8M_P$ [28,40]. All corner joint models met the drift angle accumulation criteria of 0.04 rad and the required bending moment capacity (except S3 with a 0.92 ratio). While model S3 met the specified requirements for rotation angle accumulation of at least 0.04 rad, the corresponding value of the bending capacity ratio did not meet the SMF criteria. Similarly, models S6 (1.25, 1.88), S2 (1.75, 1.19), and S5 (1.25, 1.18) demonstrated a greater tendency to resist seismic loads. Thus, beam lengths significantly affected the joint seismic performance compared to the other five specimens that were substantially safer. As shown in Table 5, all middle joint specimens met the criteria for the ultimate angle of rotation greater than 0.04 rad and the moment ratio greater than 1.30. Additionally, all interior joint models met the seismic performance criteria for SMF by having a minimum ultimate rotation angle (θ_u) of 0.05 rad and M_O (obtained moment) and $0.8M_P$ ratios greater than 1.0.

Model S6 demonstrated superior seismic performance for all joints with a maximum moments ratio of 2.0 and beams with no permanent strain distribution to columns (i.e., strong column-weak beam criteria).

Table 5
Seismic performance of joints by SMF criteria

Sp. No	Type of joint	θ_u (rad)	$\theta_{0.04}$ (rad)	M_O (kNm)	$0.8M_P$ (kNm)	$\theta_u/\theta_{0.04}$	$M_O/0.8M_P$
S1	Corner	0.05	0.04	164	142	1.25	1.15
S2	Corner	0.07	0.04	169	142	1.75	1.19
S3	Corner	0.06	0.04	130	142	1.50	0.92
S4	Corner	0.05	0.04	163	142	1.25	1.15
S5	Corner	0.05	0.04	167	142	1.25	1.18
S6	Corner	0.05	0.04	130	69	1.25	1.88
S1	Middle	0.05	0.04	438	284	1.25	1.54
S2	Middle	0.05	0.04	450	284	1.25	1.58
S3	Middle	0.05	0.04	385	284	1.25	1.36
S4	Middle	0.04	0.04	480	284	1.00	1.69
S5	Middle	0.06	0.04	485	284	1.50	1.71
S6	Middle	0.05	0.04	299	139	1.25	2.15
S1	Interior	0.05	0.04	877	568	1.25	1.54
S2	Interior	0.05	0.04	896	568	1.25	1.58
S4	Interior	0.05	0.04	825	568	1.25	1.45
S5	Interior	0.06	0.04	992	568	1.50	1.75
S6	Interior	0.05	0.04	556	278	1.25	2.00
Mean						1.30	1.52

5.4. Bending behaviour of MSB

5.4.1. Two-storey small-scale modular block

The displacement-controlled loading was applied to the top ceiling beam of the two-storey small-scale modular block fixed at the base to analyse the lateral bending efficiency of the joint. Tenons at the top and the bottom of the modular block were not passed through the lower and upper connection components. The modular block demonstrated a high bearing capacity, decent force transmission behaviour and initial stiffness of over 17 kN/mm, as illustrated in Fig.9(g). As illustrated in Fig. 10(d), the developed joint exhibits a superior force distribution tendency between the structural components of the same modular unit and the adjacent modular units. All the columns on the bottom and beams on the two welded ends showed maximum stress concentration with a load restriction. On the other hand, the bottom-storey beams exhibited no stress concentration due to their fixed boundary conditions in both longitudinal and transverse directions. It was noted that ceiling beams along the longer directions of a modular block posed the most significant risk of failure.

5.5. Parametric study on the bending behaviour of joint

5.5.1. Length of column tenon

Five corner joint models with column tenon lengths of 0, 100, 200, 300, and 400 mm were chosen to investigate the effect of column tenon on the joint's bending behaviour. As illustrated in Figs. 8(a) and (f), increasing the length of the column tenon increased both bending capacities and stiffnesses. Although capacity and stiffness were raised, the rise was decreased by 25, 16, 11, and 10%, and 38, 21, 12, and 9%. With a strong column-weak beam pattern, increasing the length of the column tenon increased the moment capacity and stiffness. Additionally, models with tenon lengths of 0 and 100 mm demonstrated unsatisfactory seismic performance, whereas models with tenon

lengths of 200, 300, and 400 mm demonstrated satisfactory seismic performance.

5.5.2. Length of beam tenon

Four corner joint models with beam tenon lengths of 0, 100, 200, and 300 mm revealed a slight increase (<5%) in bending capacity and stiffness as beam tenon length increased, as shown in Fig. 8(b) and (g).

5.5.3. Thickness of gusset plate (GP)

Four different GP thicknesses were chosen, such as 20, 30, 40, and 50 mm, to investigate GP thickness effect on the joint's structural performance. There was no distinguishable increase in capacity, stiffness, or seismic performance was observed as the thickness of GP was increased, as shown in Fig. 8© and (h).

5.5.4. Thickness of beams

On average, beams (FB and CB) of three different thicknesses (i.e., 6, 8, and 10 mm) increased the capacity and stiffness of the joint by 5%, as shown in Fig. 8(d) and (i). Additionally, the model with the most significant beam thickness exhibited plastic deformation only in the column (model S1), whereas the model with the most negligible beam thickness also exhibited an accumulation of plastic strain in the beams.

5.5.5. Inter-modular gap

The bending moment of four models of middle joint with an inter-modular gap of 20, 40, 60, and 80 mm were compared to determine the effect of the constructional gap on the lateral performance of joints. A nonapparent rise in a moment carrying capacity and stiffness (<5%) was illustrated in Figs. 8(e) and (j), whereas permanent strain accumulation was only limited to beams.

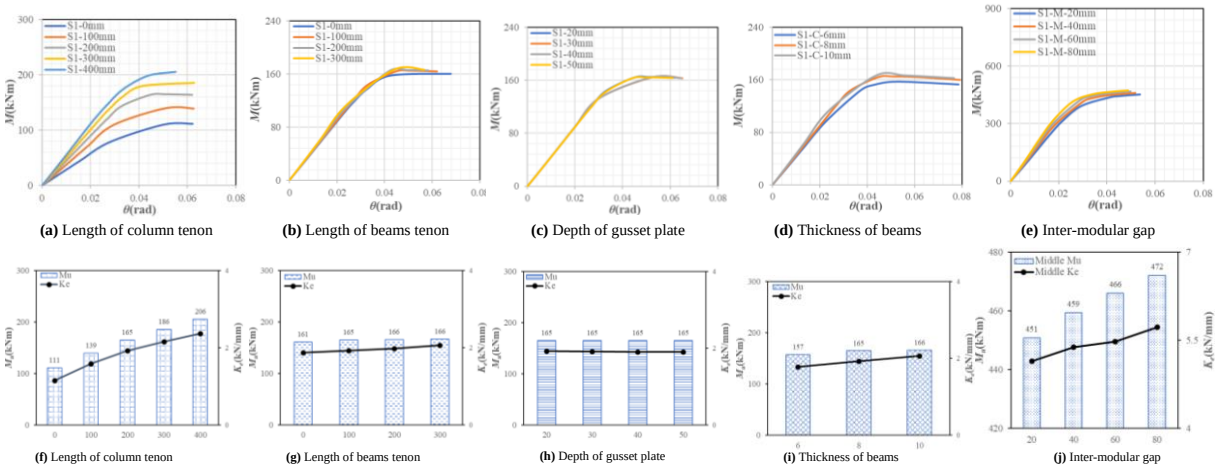

(a) Length of column tenon **(b)** Length of beams tenon **(c)** Depth of gusset plate **(d)** Thickness of beams **(e)** Inter-modular gap

(f) Length of column tenon **(g)** Length of beams tenon **(h)** Depth of gusset plate **(i)** Thickness of beams **(j)** Inter-modular gap

Fig. 8 Parametric studies on the lateral behaviour of joints

5.6. Simplification of joint

To save considerable computational time and accurately simulate the elastoplastic behaviour of a solid model of the joints, a beam model based on nonlinear spring connectors and beam elements was developed. The deformable solid elements of structural members, such as beams and columns, were replaced with three-dimensional beam elements, and the detailed joint model was replaced with nonlinear spring connectors. The connector's rotational stiffness was determined using the momentum versus rotation curves generated by the detailed FE model. Boundary conditions, material properties, cross-section characteristics, and loading conditions were maintained in the same way as the detailed FE analysis. Fig. 9 illustrates the comparison of the eighteen detailed and developed simplified joint models of the corner, middle, and interior joints and a two-storey modular block. It is worth noting that the curves obtained from simplified models accurately predicted the elastic stiffness, ultimate capacity, and plastic behaviour of detailed models, except for model S3, which failed to converge when detailed solid element modelling was used. Table 6 compares the ultimate moments of detailed and simplified FE models and evaluates mean and Cov, which indicates that the mean and Cov are 0.99 and 0.025, respectively. Additionally, the table summarises the moment capacities of detailed-to-simplified models using moment ratios $\left(\frac{M_{Det}}{M_{Sim}}\right)$. It indicated that when the ratios exceed 1.0, the simplified model was slightly underestimated, implying that structural behaviour predictions are safe. In comparison, ratios less than 1.0 indicate that actual behaviour is overestimated by simplified models, implying that structural behaviour estimations are slightly unsafe. These comparisons of moment-rotation curves and predicted moment ratios demonstrate that a simplified beam and connector model can accurately simulate the lateral behaviour of developed joints in MSB when both axial compression and lateral loading are applied. Additionally, Fig. 10 compares the stresses contours of the corresponding models. It was demonstrated that the simplified model accurately predicted the developed joints' structural behaviour and failure initiation. As a result of their accuracy, prediction of nonlinear structural behaviour, and increased computational efficiency, these simplified models are recommended for practical applications.

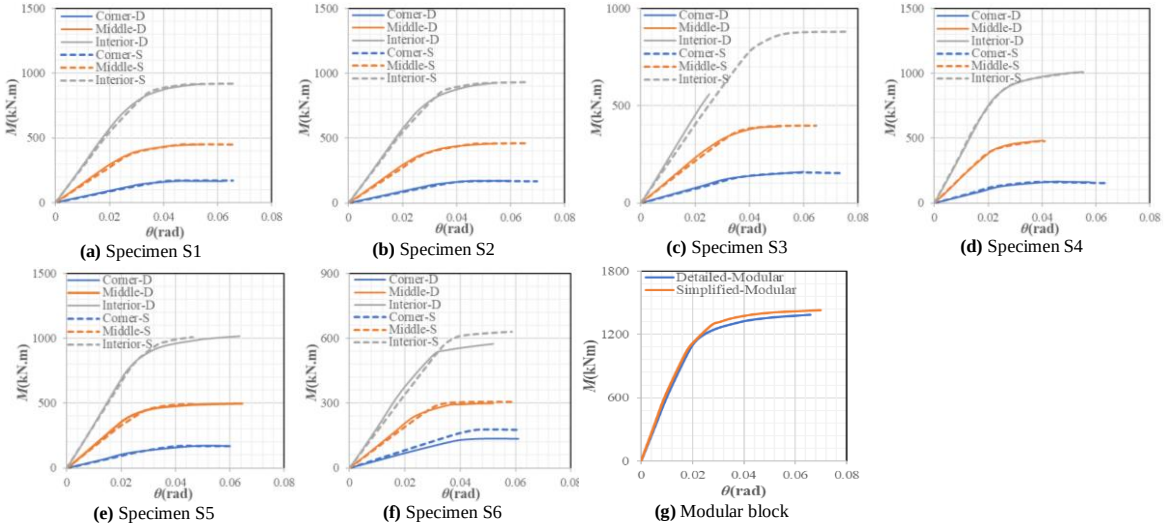

(a) Specimen S1 **(b)** Specimen S2 **(c)** Specimen S3 **(d)** Specimen S4

(e) Specimen S5 **(f)** Specimen S6 **(g)** Modular block

Fig. 9 Comparison of moment-rotation curves of detailed (D) and simplified (S) FE models

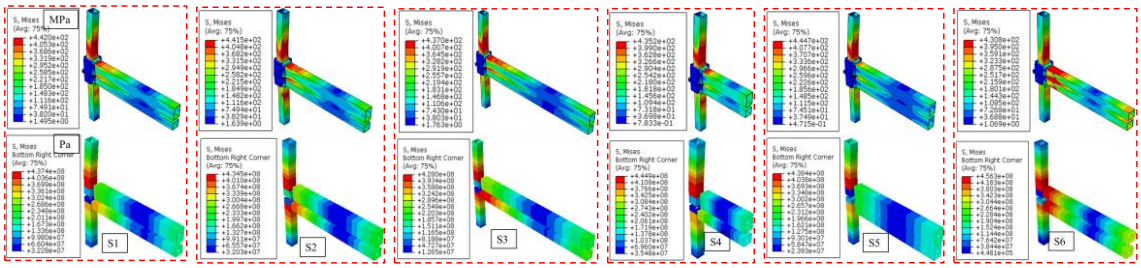

(a) FE models of corner joint

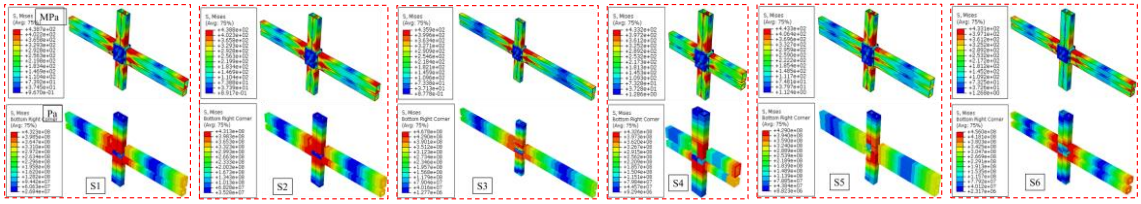

(b) FE models of middle joint

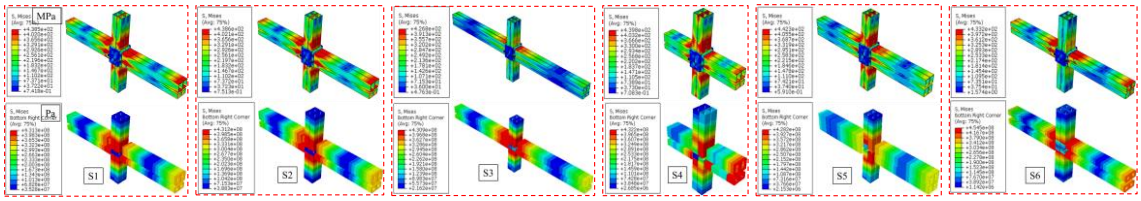

(c) FE models of interior joint

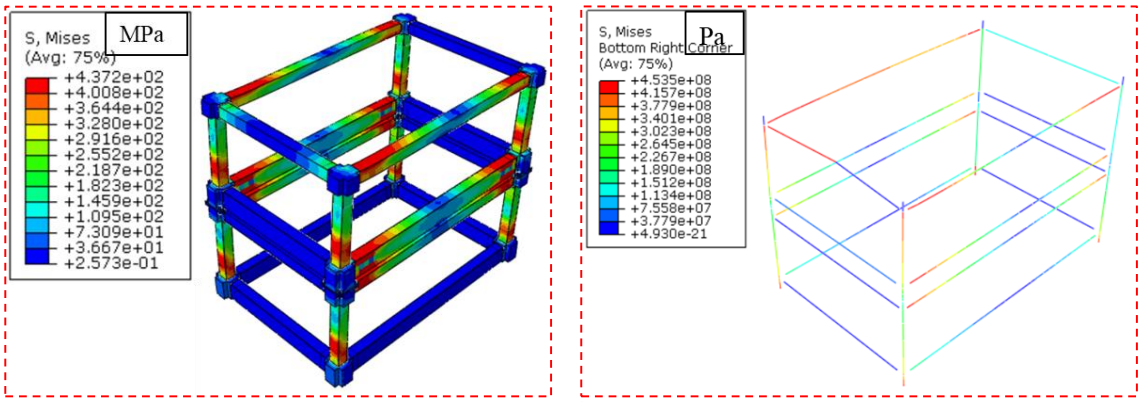

(d) FE models of two-storey modular block

Fig. 10 Comparison of stress distribution of detailed (D) and simplified (S) FE models

Table 6
Comparison of ultimate capacities of detailed and simplified FE models

Sp. No	Type of joint	Ultimate moment $M_{Detailed}$(kNm)	Ultimate moment $M_{Simplified}$(kNm)	M_{Det}/M_{Sim}
S1	Corner	165	168	0.98
S2	Corner	172	171	1.00
S3	Corner	159	155	1.02
S4	Corner	164	163	1.00
S5	Corner	167	170	0.98
S6	Corner	174	179	0.97
S1	Middle	450	448	1.00
S2	Middle	460	459	1.00
S3	Middle	393	398	0.98
S4	Middle	479	476	1.00
S5	Middle	497	491	1.01
S6	Middle	301	306	0.98
S1	Interior	918	919	0.99
S2	Interior	927	931	0.99
S4	Interior	1009	1006	1.00
S5	Interior	1018	1009	1.00
S6	Interior	573	630	0.90
Block	Block	1389	1428	0.97
Mean				0.99
Cov				0.025

6. Discussions

Previous research has emphasised the critical role of joints as a lateral force-resistant system in ensuring the integral and reliable nature of MSBs during catastrophic events. [14–16]. As reported in the literature, the present study proposed a joint for SHS, as illustrated in Fig. 1, to avoid the use of weaker sections, drilling holes in sections, sacrificing aesthetics, and stiffening joints. Fig. 6 shows the lateral bending capacity of joints. The procedure for determining the bending capacity of each joint was identical to that reported previously [17,28,31,32]. The developed joints were found to have a significantly higher lateral load-carrying capacity and seismic response than previously proposed joints [41,42]. According to previous research, semi-rigid frames with a drift ratio greater than 0.032 rad were found appropriate for use in earthquake-prone zones [43]. In comparison, the American Steel Construction Institute's (AISC) seismic provisions require that the lowest possible drift ratio by joints in special moment frames (SMF) be larger than 0.04 rad for capacities greater than $0.8M_p$ [40]. As shown in Table 5, the developed joints fulfilled high seismic performance requirements with $\theta_u/\theta_{0.04} \geq 1$ and $M_O/0.8M_P \geq 1$ and can be used as a lateral force resistant system in MSB. Increased column tenon length resulted in superior seismic performance of the joint (with $\theta_u/\theta_{0.04} \geq 1$ and $M_o/0.8M_P \geq 1$). At the corresponding rotational angle, the corner joint with a tenon length of 0 or 100 mm did not meet current requirements, but the models with a length of 200, 300, or 400 mm met AISC criteria for use in SMF.

The strength, i.e., $0.25M_P \leq M_j \leq M_P$ and stiffness classification criteria, i.e., $0.5EI_b/L_b \leq S_{ji} \leq 25EI_b/L_b$ for the unbraced semi-rigid frames used in the study, have been widely adopted previously [44,45]. According to the criteria, the corner joint with a single FB exhibited semi-rigid behaviour with strength $>0.5M_P$ and a rotational stiffness $>0.5EI_b/L_b$. The middle and interior joints with two and four FBs behaved as rigid joints in the strength classification with strength $>M_P$ and semi-rigid with rotational stiffness $>0.5EI_b/L_b$, except for S6. Such variations in joint behaviour due to beam length and the effect of adjacent modular units on strength and stiffness had received less attention; therefore, a detailed study was conducted in this context. Previously published research has demonstrated the contribution of shear walls, different loading scenarios, and the impact of wall openings on the response and rigidity of modular units [46–48]. On the other hand, the participation of joints in the overall lateral effectiveness of modular units received relatively less attention. The results of the specific bending analysis indicated that when the members' strengths were adequately utilised, the joint in a double-storey module acquired a greater tendency for bearing lateral loads [38]. Previous studies examined simplified models of multistorey modular frames, but there was no stepwise simplified representation and affirmation of the models' appropriateness [8,30]. Likewise, the developed simplified models of joints could simulate only elastic responses with a wide range of plastic regime variation. As illustrated in Fig. 9 and 10, the current study validated the step-by-step comparative efficacy of simplified models and their effectiveness in stimulating the complex detailed models.

7. Conclusions

This study aimed to develop new joints in MSB for SHS members, addressing issues with previously established joints. A detailed 3D FE analysis was performed to simulate the bending performance of the developed joints. Then, in-depth parametric analyses were performed to determine the effect of various parameters on the joints' overall structural performance. Simultaneously, the response of the developed joint in the two-storey small-scale modular block was investigated to mimic its contribution in multistorey MSB. Following that, joints were simplified using connector and beam elements to predict the elastoplastic response of complex joints. Finally, the FE modelling accuracy was confirmed by comparing it to thirteen tests on MSB joints. These studies on joints and a modular block justify the following conclusions:

1) Comparing FE results to thirteen joint bending tests revealed that the developed FE models accurately captured initial stiffness, ultimate bearing capacity, and failure behaviour.
2) The stiffness, lateral capacity, seismic performance, and ductility of the corner, middle, and inner joints were adequate. Beam tenons, GP thickness, and the intermodular gap had no noticeable impact on capacity and stiffness, whereas column tenon length had a significant influence. Beam failure was observed in models with longer and smaller cross-section beams. Columns from middle and inner joints and models of corner joints with weaker beams demonstrated strong-column and weak-beam responses, making them consistent with successful seismic behaviour.
3) The modular block showed a stable lateral load-carrying capacity, rotational stiffness, load distribution, and ductility. The ceiling beams of the upper storey were permanently deformed, but the columns remained safe, meeting strong-column and weak-beam criteria for adequate seismic behaviour.
4) By accurately simulating the elastoplastic behaviour and ultimate bearing capacity of detailed models with a Cov of 0.025, the development of simplified joints with nonlinear spring connector and beam element reduced modelling effort and increased computational efficiency.

Acknowledgment

The authors gratefully acknowledge the research grant received from the China Postdoctoral Science Foundation (Grant No. 2020M670655), the National Natural Science Foundation of China (Grant No. 51978457), and the Science and Technology Project of Tianjin (Grant No. 17ZXCXSF00050). The authors would like to express their profound gratitude for the financial support. The authors would also like to acknowledge the China Scholarship Council for funding the first author's studies at Tianjin University in China.

Nomenclature

σ_T= True stress
σ_E= Engineering stress
ε_E= True strain
ε_T=Engineering strain
E_s= Steel's modulus of elasticity
N= Axial force
A_s= Cross-section are
A_e= Bolts effective area
f_{tv}= Bolts tensile strength
σ_{EQ}= Equivalent stress
σ_1, σ_2 and σ_3= Principal stresses
$\dot{\varepsilon}_{ij}^{p}$= Rate of plastic strain
M_O= Obtained moment
M_P= Plastic moment
K_e= Initial/elastic stiffness
d_b= Diameter of bolt
$\frac{M_{Det}}{M_{Sim}}$= Moment capacities ratios of detailed and simplified models
P= Pretension of a bolt
Δ= Lateral displacement
θ= Rotation angle (rad)
μ= Coefficient of friction
P_{Test}= Ultimate strength of test specimens
P_{FE}= Ultimate strengths of FE models
ν= Poisson's ratio
f_y= Yield strength
f_u= Ultimate strength

References

[1] Smith RE. Prefab Architecture: A Guide to Modular Design and Construction. 2011. https://doi.org/10.1017/CBO9781107415324.004.
[2] Alembagheri M, Sharafi P, Hajirezaei R, Samali B. Collapse capacity of modular steel buildings subject to module loss scenarios: The role of inter-module connections. Eng Struct 2020;210. https://doi.org/10.1016/j.engstruct.2020.110373.
[3] Lawson M, Ogden R, Goodier C. Design in Modular Construction. 2014. https://doi.org/10.1201/b16607.
[4] Kamali M, Hewage K. Life cycle performance of modular buildings: A critical review. Renew Sustain Energy Rev 2016;62:1171–83. https://doi.org/10.1016/j.rser.2016.05.031.
[5] Sharafi P, Mortazavi M, Samali B, Ronagh H. Interlocking system for enhancing the integrity of multi-storey modular buildings. Autom Constr 2018;85:263–72. https://doi.org/10.1016/j.autcon.2017.10.023.
[6] Jiang R, Mao C, Hou L, Wu C, Tan J. A SWOT analysis for promoting off-site construction under the backdrop of China's new urbanisation. J Clean Prod 2018;173:225–34. https://doi.org/10.1016/j.jclepro.2017.06.147.
[7] Lacey AW, Chen W, Hao H, Bi K. Review of bolted inter-module connections in modular steel buildings. J Build Eng 2019;23:207–19. https://doi.org/10.1016/j.jobe.2019.01.035.
[8] Annan CD, Youssef MA, El Naggar MH. Seismic vulnerability assessment of modular steel buildings. J Earthq Eng 2009;13:1065–88. https://doi.org/10.1080/13632460902933881.
[9] Zhang JF, Zhao JJ, Yang DY, Deng EF, Wang H, Pang SY, et al. Mechanical-property tests on assembled-type light steel modular house. J Constr Steel Res 2020;168:105981. https://doi.org/10.1016/j.jcsr.2020.105981.
[10] Lawson RM, Ogden RG, Bergin R. Application of Modular Construction in High-Rise Buildings. J Archit Eng 2012;18:148–54. https://doi.org/10.1061/(ASCE)AE.1943-5568.0000057.
[11] Jellen AC, Memari AM. The state-of-the-art application of modular construction to multi-story. 1st Resid Build Des Constr Conf 2013:284–93.

[12] Lacey AW, Chen W, Hao H, Bi K. Structural response of modular buildings – An overview. J Build Eng 2018;16:45–56. https://doi.org/10.1016/j.jobe.2017.12.008.
[13] Liew JYR, Chua YS, Dai Z. Steel concrete composite systems for modular construction of high-rise buildings. Structures 2019:0–1. https://doi.org/10.1016/j.istruc.2019.02.010.
[14] Lawson PM, Byfield MP, Popo-Ola SO, Grubb PJ. Robustness of light steel frames and modular construction. Proc Inst Civ Eng Struct Build 2008;161:3–16. https://doi.org/10.1680/stbu.2008.161.1.3.
[15] Ding Y, Deng EF, Zong L, Dai XM, Lou N, Chen Y. Cyclic tests on corrugated steel plate shear walls with openings in modularized-constructions. J Constr Steel Res 2017;138:675–91. https://doi.org/10.1016/j.jcsr.2017.08.019.
[16] Chua YS, Liew JYR, Pang SD. Robustness of Prefabricated Prefinished Volumetric Construction (PPVC) High-rise Building 2018. https://doi.org/10.4995/asccs2018.2018.6955.
[17] Cho BH, Lee JS, Kim H, Kim DJ. Structural performance of a new blind-bolted frame modular beam-column connection under lateral loading. Appl Sci 2019;9. https://doi.org/10.3390/app9091929.
[18] Sanches R, Mercan O, Roberts B. Experimental investigations of vertical post-tensioned connection for modular steel structures. Eng Struct 2018;175:776–89. https://doi.org/10.1016/j.engstruct.2018.08.049.
[19] Deng EF, Zong L, Ding Y, Dai XM, Lou N, Chen Y. Monotonic and cyclic response of bolted connections with welded cover plate for modular steel construction. Eng Struct 2018;167:407–19. https://doi.org/10.1016/j.engstruct.2018.04.028.
[20] Azizi Naserabad A, Ghasemi MR, Shabakhty N, Ghohani Arab H. Design of a Novel Prefabricated Bolted I-Beam to Box-Column Connection Using Numerical Analysis Under Cyclic Load. Int J Steel Struct 2019;19:1431–45. https://doi.org/10.1007/s13296-019-00222-6.
[21] Azizi Naserabad A, Ghasemi MR, Shabakhty N, Ghohani Arab H. Evaluation of Three Support Shapes on Behavior of New Bolted Connection BBCC in Modularized Prefabricated Steel Structures. Int J Steel Struct 2018;18:1639–53. https://doi.org/10.1007/s13296-018-0051-9.
[22] Dhanapal J, Ghaednia H, Das S, Velocci J. Structural performance of state-of-the-art VectorBloc modular connector under axial loads. Eng Struct 2019;183:496–509. https://doi.org/10.1016/j.engstruct.2019.01.023.
[23] Dhanapal J, Ghaednia H, Das S, Velocci J. Behavior of thin-walled beam-column modular connection subject to bending load. Thin-Walled Struct 2019:106536. https://doi.org/10.1016/j.tws.2019.106536.
[24] Khan K, Yan J-B. Numerical studies on seismic behaviour of a prefabricated multi storey modular steel building with new type bolted joints. Adv Steel Constr n.d.;17(1):1–9. https://doi.org/10.18057/IJASC.2021.17.1.1.
[25] Khan K, Yan J-B. Development and Study on the Seismic Behavior of Novel Joint in Pre-fabricated Modular Steel Building. Tianjin University, 2017. https://doi.org/10.1017/CBO9781107415324.004.
[26] Khan K, Yan JB. Finite Element Analysis on Seismic Behaviour of Novel Joint in Prefabricated Modular Steel Building. Int J Steel Struct 2020. https://doi.org/10.1007/s13296-020-00320-w.
[27] Zuo Y, Zha X. FEM and Experimental Study on Mechanical Property of Integrated Container Building. Int J Steel Struct 2018;18:699–718. https://doi.org/10.1007/s13296-018-0065-3.
[28] Lee S, Park J, Kwak E, Shon S, Kang C, Choi H. Verification of the seismic performance of a rigidly connected modular system depending on the shape and size of the ceiling bracket. Materials (Basel) 2017;10. https://doi.org/10.3390/ma10030263.
[29] Annan CD, Youssef M, Naggar MH. Seismic performance of modular steel braced frames. 9h Can Conf Earthq Eng 2007. https://doi.org/10.13140/2.1.2132.2241.
[30] Fathieh A, Mercan O. Seismic evaluation of modular steel buildings. Eng Struct 2016;122:83–92. https://doi.org/10.1016/j.engstruct.2016.04.054.
[31] Chen Z, Liu J, Yu Y, Zhou C, Yan R. Experimental study of an innovative modular steel building connection. J Constr Steel Res 2017;139:69–82. https://doi.org/10.1016/j.jcsr.2017.09.008.
[32] Chen Z, Liu J, Yu Y. Experimental study on interior connections in modular steel buildings. Eng Struct 2017;147:625–38. https://doi.org/10.1016/j.engstruct.2017.06.002.
[33] Chen Z, Liu Y, Zhong X, Liu J. Rotational stiffness of inter-module connection in mid-rise modular steel buildings. Eng Struct 2019;196:109273. https://doi.org/10.1016/j.engstruct.2019.06.009.
[34] ABAQUS (2013). User manual Version 6.13. DS SIMULIA Corp, Provid RI, USA 2013:1–847.
[35] Yan J-B. Finite element analysis on steel–concrete–steel sandwich beams. Mater Struct 2015;48:1645–67. https://doi.org/10.1617/s11527-014-0261-3.
[36] Chen Z, Xu J, Chen Y, Xue J. Axial compression ratio limit values for steel reinforced concrete (SRC) special shaped columns. Steel Compos Struct 2016;20:295–316. https://doi.org/10.12989/scs.2016.20.2.295.
[37] ASCE/SEI. ASCE STANDARD Loads for Buildings. Virginia: 2010.
[38] Chen Z, Li H, Chen A, Yu Y, Wang H. Research on pretensioned modular frame test and simulations. Eng Struct 2017;151:774–87. https://doi.org/10.1016/j.engstruct.2017.08.019.
[39] Yan JB, Chen Y, Lin X. Finite element analysis and parametric studies on hysteretic behaviours of high strength steel T-joints with damage-control fuses. Thin-Walled Struct 2020;148. https://doi.org/10.1016/j.tws.2019.106574.
[40] ANSI/AISC 341-16. Seismic Provisions for Structural Steel Buildings. 2016. https://doi.org/10.1201/b11248-8.
[41] Sup S, Woong K, Sung K, Yub S. An Experimental Evaluation of Structural Performance for the Beam to Column Joints in Unit Modular System. J Korean Soc Steel Constr 2013;25:255–65. https://doi.org/10.7781/kjoss.2013.25.3.255.
[42] Lee. Behavior of C-Shaped Beam to Square Hollow Section Column Connection in Modular Frame. J Korean Soc Steel Constr 2015;27:471. https://doi.org/10.7781/kjoss.2015.27.5.471.
[43] Liu XC, Pu SH, Zhang AL, Xu AX, Ni Z, Sun Y, et al. Static and seismic experiment for bolted-welded joint in modularized prefabricated steel structure. J Constr Steel Res 2015;115:417–33. https://doi.org/10.1016/j.jcsr.2015.08.036.
[44] EN 1993-1-1. Eurocode 3: Design of steel structures - Part 1-1: General rules and rules for buildings. vol. 1. 2011.
[45] Choi K-S, Kim H-J. Analytical Models of Beam-Column joints in a Unit Modular Frame. J Comput Struct Eng Inst Korea 2014;27:663–72. https://doi.org/10.7734/coseik.2014.27.6.663.
[46] Zuo Y, Zha X. FEM and experimental study on mechanical property of container building with holes. Int J Steel Struct 2017;17:175–94. https://doi.org/10.1007/s13296-015-0132-y.
[47] Yu Y, Chen Z. Rigidity of corrugated plate sidewalls and its effect on the modular structural design. Eng Struct 2018;175:191–200. https://doi.org/10.1016/j.engstruct.2018.08.039.
[48] Giriunas K, Sezen H, Dupaix RB. Evaluation, modeling, and analysis of shipping container building structures. Eng Struct 2012;43:48–57. https://doi.org/10.1016/j.engstruct.2012.05.001.